Front. Environ. Sci. Eng. 2021, 15(6): 132
https://doi.org/10.1007/s11783-021-1425-3

RESEARCH ARTICLE

A Cu-modified active carbon fiber significantly promoted H_2S and PH_3 simultaneous removal at a low reaction temperature

Yingwu Wang[1], Ping Ning[1], Ruheng Zhao[1], Kai Li (✉)[1], Chi Wang[2], Xin Sun[1], Xin Song[1], Qiang Lin (✉)[1,3]

1 Faculty of Environmental Science and Engineering, Kunming University of Science and Technology, Kunming 650500, China
2 Faculty of Chemical Engineering, Kunming University of Science and Technology, Kunming 650500, China
3 Hainan Normal University, Haikou 571158, China

HIGHLIGHTS

- $Cu_{0.15}$-ACF performs the best for H_2S and PH_3 simultaneous removal.
- 550°C and 90°C are separately calcination and reaction temperatures.
- The reason why $Cu_{0.15}$/ACF shows better performance was found.
- The accumulation of $H_2PO_4^-$ and $SO_4^{2-}(H_2O)_6$ is the deactivation cause of $Cu_{0.15}$/ACF.

GRAPHIC ABSTRACT

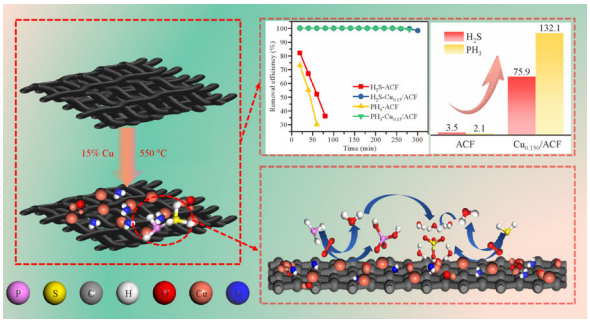

ARTICLE INFO

Article history:
Received 6 July 2020
Revised 27 January 2021
Accepted 10 February 2021
Available online 10 April 2021

Keywords:
ACF
H_2S
PH_3
Cu
Low temperature
Simultaneous removal

ABSTRACT

Poisonous gases, such as H_2S and PH_3, produced by industrial production harm humans and damage the environment. In this study, H_2S and PH_3 were simultaneously removed at low temperature by modified activated carbon fiber (ACF) catalysts. We have considered the active metal type, content, precursor, calcination, and reaction temperature. Experimental results exhibited that ACF could best perform by loading 15% Cu from nitrate. The optimized calcination temperature and reaction temperature separately were 550°C and 90°C. Under these conditions, the most removal capacity could reach 69.7 mg/g and 132.1 mg/g, respectively. Characterization results showed that moderate calcination temperature (550°C) is suitable for the formation of the copper element on the surface of ACF, lower or higher temperature will generate more cuprous oxide. Although both can exhibit catalytic activity, the role of the copper element is significantly greater. Due to the exceptional dispersibility of copper (oxide), the ACF can still maintain the advantages of larger specific surface area and pore volume after loading copper, which is the main reason for better performance of related catalysts. Finally, increasing the copper loading amount can significantly increase the crystallinity and particle size of copper (oxide) on the ACF, thereby improving its catalytic performance. *In situ* IR found that the reason for the deactivation of the catalyst should be the accumulation of generated $H_2PO_4^-$ and $SO_4^{2-}(H_2O)_6$ which could poison the catalyst.

1 Introduction

As highly toxic gases, hydrogen sulfide (H_2S) and phosphine (PH_3) are the common exhaust gases in the phosphorous chemical industry (Stita et al., 2015), which can poison the catalysts for high-valued CO recycle (Ma et al., 2008). The untreated emission of H_2S and PH_3 is also harmful to human health and the environment (Abdolghaffari et al., 2015). Hence, a strong motivation is necessary for removing these pollutants simultaneously. The corona discharge non-thermal plasma (NTP) achieved the simultaneous removal of PH_3 and H_2S in a wire-cylinder reactor (Ma et al., 2016). Higher specific input energy (SIE) was good for promoting conversion rate while there was a problem of relatively low energy utilization. Also, biological methods were used for the purification of H_2S (Ma et al., 2016) or PH_3 (Deng et al.,

✉ Corresponding authors
E-mail: likaikmust@163.com (K. Li); linqiangkmust@163.com (Q. Lin)

2013). However, they performed poorly at high concentrations comparing to the adsorption oxidation method. The wet adsorption oxidation, such as modified manganese slag slurry (Sun et al., 2020), performed much better in the removal of high concentration H_2S and PH_3. While the samples or catalysts are difficult to characterize, recover, and regenerate, the reaction process is also difficult to analyze. The dry adsorption oxidation method (gas-solid reaction) could solve that problem well and had been widely reported (Wang et al., 2018; Liu et al., 2020). Also, low temperature (< 200°C) and low oxygen concentration of the tail gas have been considered here. Therefore, the method of low-temperature adsorption oxidation has been used for H_2S and PH_3 simultaneous removal in this study.

The choice of materials is another important point in addition to the method. Here, we focused on the activated carbon fiber (ACF) which has attracted lots of attention in the pollutant control area due to high specific surface area and functional groups (Bai et al., 2017). The production of ACF from lower cost precursors, such as agricultural wastes, has been suggested by the researcher. (Lee et al., 2014). Transition metal oxides, such as MnO_2, CeO_2 (Gu et al., 2019) and Fe_2O_3, TiO_2, CuO_x (Kim and Lee, 2018; Hou et al., 2019), are also widely used to modify ACF for improving its capacity (Lan et al., 2015) by changing textural and chemical properties (de Falco et al., 2018). Transition metal oxides have a variety of surface structures, which affect the surface energy and chemical properties of themselves. The coordination mode of surface metal cations and oxygen anions will also affect the acidity and basicity of the catalyst and its catalytic performance (Xu et al., 2020).

Herein, we have investigated the type and concentration of transition metal oxides as well as the reaction and calcination temperature according to their performance for simultaneous removal of H_2S and PH_3. Furthermore, the properties of adsorbents were characterized and analyzed by Brunauer-Emmett-Teller (BET), Scanning Electronic Microscopy (SEM), X-ray diffraction (XRD), and *in situ* Infrared Reflectance (IR).

2 Experimental

2.1 Catalyst preparation

The traditional impregnation method was used to prepare the catalysts used in this paper. The ACF was purchased from Nantong Senyou Carbon Fiber Company, located in Jiangsu, China. It was first ground into a powder with 40–60 meshes, washed with deionized (DI) water several times to remove the dust, and then dried at 100°C for 24 h. Then, the ACF, metal nitrate, and deionized water was mixed and stirred up for 2 h. After drying at 100°C for over 12h, the powder was calcined at temperature (T) for 1h in 10°C/min with nitrogen gas flow protection. The ratio from M to ACF was X which equaled 2.5%, 5%, 7.5%, 10%, 12.5%, 15%, 20%. The ratio of ACF to DI water was 1g: 10 mL in the whole process. The precursors, SO_4^{2-}, Cl^-, CH_3COO^-, and NO_3^- were chosen to test based on the same content of transition metal. The final catalyst has been defined as M_x / ACF@[T], where M (= Cu, Fe, Mn, Zn, Ni, Co) was the elemental metal from metal salt and T (= 350°C, 450°C, 550°C, 650°C, and 750°C) was the calcination temperature.

2.2 Experimental evaluation

A10 mm fixed-bed quartz reactor with 0.5 g catalyst was used for all activity tests. Other conditions were as follows: the weight hourly space velocity (WHSV) was approximately 36000 mL/(g·h); concentrations were 0.46 mg/L H_2S, 0.91 mg/L PH_3, and 0.5% O_2; N_2 was used as the balance gas (Wang et al., 2018). FULI gas chromatography analyzer was employed to measure the concentrations of H_2S and PH_3 in the gases. The performance of catalysts was judged based on removal efficiency and capacity, which was calculated using Eqs. (1) and (2), respectively (Wang et al., 2018).

$$\mathrm{H_2S(PH_3)\ removal\ efficiency(\%)} = \frac{[\mathrm{H_2S(PH_3)}]_{\mathrm{inlet}} - [\mathrm{H_2S(PH_3)}]_{\mathrm{outlet}}}{[\mathrm{H_2S(PH_3)}]_{\mathrm{inlet}}} \times 100 \quad (1)$$

$$\mathrm{H_2S(PH_3)\ removal\ capacity(\%)} = \frac{Q\int_0^t (C_{\mathrm{inlet}} - C_{\mathrm{outlet}})\mathrm{d}t}{m} \quad (2)$$

where Q is total flow rate; t is reaction time; C_{inlet} is inlet concentration of H_2S or PH_3; C_{outlet} is outlet concentration of H_2S or PH_3; m is catalyst mass.

2.3 Catalyst characterization methods

The adsorption-desorption isotherms of the catalysts were measured through a surface-area analyzer (BELSORP-max, BEL, Japan; IQ2, Quantachrome, USA). All samples were degassed at 300°C for 5 h. The BET and BJH methods were used to analyze specific surface area and pore-size distributions, respectively. X-ray diffraction (XRD) was obtained using an X-ray diffractometer (UltimaIV Cu Ka radiation diffractometer, Japan) equipped with a rate of 5°/min from 2θ = 10°–80° (λ = 0.15406 nm, V = 40 KV, I = 40 mA). The JCPDS file was adopted to mark the crystalline phases of catalysts. The MDI jade 6.0 was used to calculate crystallinity. *In situ* FTIR analysis was performed on an infrared spectrophotometer (Avater 360, Nicolet, USA) with scanning 32 times from 400 to 4000 cm^{-1} by the instrument resolution

was 4 cm^{-1}. Field-emission scanning electron microscopy (FESEM) images were measured under different resolutions (Nova NanoSEM 450).

3 Results and discussion

3.1 Experiments results

3.1.1 Influence of the calcination temperature

The $Cu_{0.05}$/ACF, calcinated under the temperature range 350°C to 750°C, has been used to discuss the influence of calcination temperature through comparing their performance. Results and removal capacity have been shown in Fig. 1. The removal efficiency of H_2S and PH_3 initially increased and then decreased with increasing calcination temperature. The best performance occurred at 550°C, which is shown in Figs. 1(a) and 1(b). The duration of 100% H_2S and PH_3 removal could be 60 and 40 min, respectively. Figure 1(c) displayed that the removal capacity of H_2S (37.1 mg/g) and PH_3 (66.7 mg/g) individually increased by 50% and 58% with the calcination temperature rising from 350°C to 550°C. Once over 550°C, there was a dramatic decline in the performance and removal capacity of $Cu_{0.05}$/ACF. Because AC composited materials with high surface areas that were slightly affected by calcination temperature, the main rationale explaining this phenomenon is that the higher calcination temperature affect the active component (Zhao et al., 2016).

3.1.2 Influence of transition metal oxides and precursors

The $M_{0.05}$/ACF catalysts (M = Cu, Fe, Mn, Zn, Ni, and Co) loaded by different transition metal (oxides) have been tested for H_2S and PH_3 simultaneous removal. Different precursors (SO_4^{2-}, Cl^-, $(NO_3)^{2-}$, and CH_3COO^-) of chosen metal were also tested, which were affecting the structure and properties of materials (Basova et al., 2005). The results and removal capacity of the catalysts were displayed in Fig. 2.

For the factor of metals, the catalysts prepared by supporting different metals showed clear differences in the removal of H_2S and PH_3. Among them, the performance of copper ($Cu_{0.05}$/ACF) is significantly better than others, especially in the removal of PH_3 (Figs. 2(b) and 2(d)). The duration of H_2S 100% removal was 90 min and the removal capacity was 27.1 mg/g which was triple higher than that of $Mn_{0.05}$/ACF (8.9 mg/g). The time of $PH_3$100% removal was 60 min and capacity of 30.4 mg/g which was 9 times as high as that of $Mn_{0.05}$/ACF (3.8 mg/g) (Fig. 2(e)). From the precursors of Cu, the catalysts prepared from different copper sources had little effect on the removal of H_2S, and $Cu(NO_3)_2$ is slightly better than others. The effect on the removal of PH_3 is significant, of which Cu $(CH_3COO)_2$ performs the worst, and $Cu(NO_3)_2$ performs the best. The decomposition of $CuSO_4$ was incomplete at 550°C and $Cu(CH_3COO)_2$ would generate more Cu_2O, while the nitrogen and oxygen functional groups generated by NO_3^- in the roasting process could significantly improve the performance of the material (Li et al., 2016). This indicated that the copper nitrate was more suitable here to prepare catalysts for removing H_2S and PH_3 simultaneously.

3.1.3 Influence of transition metal content

The effect of Cu content was further studied and the results were presented in Fig. 3. The general trend of their removal efficiency first increased and then decreased with Cu content increasing (Figs. 3(a) and 3(b). From 5% to 7.5%, there was a huge performance improvement. It reached a peak when the Cu was increased to 15%. A further increase would negatively impact the simultaneous removal of H_2S and PH_3. The corresponding removal capacity also changed accordingly. The time that H_2S and PH_3 could be 100% removed were 300 and 250 min, respectively. The removal capacity of H_2S on $Cu_{0.15}$/ACF was 60.1 mg/g which has been increased to 4.1 times as compared with $Cu_{0.025}$/ACF (Fig. 3(c)). There was around 13.6-fold

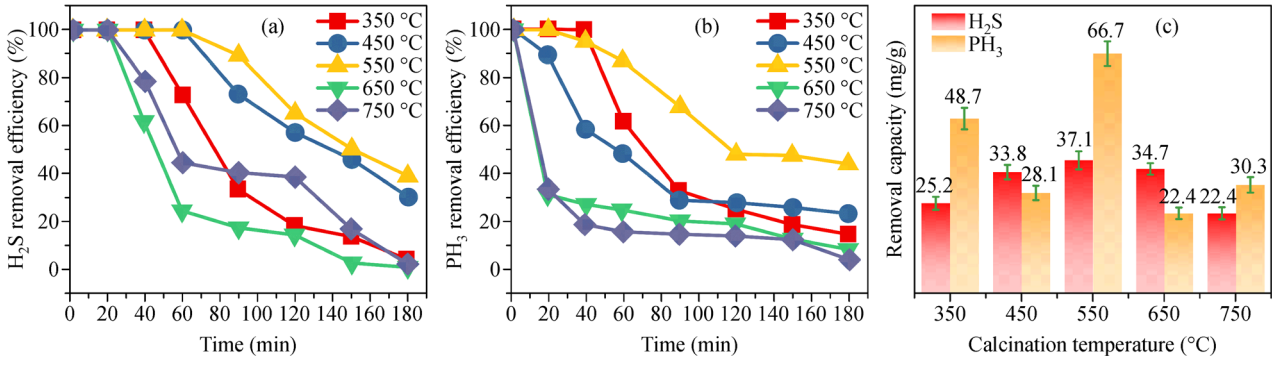

Fig. 1 The influence of calcination temperature for H_2S (a) and PH_3 (b) simultaneous removal and their removal capacity (c). Conditions: 5% metal (Cu) loading; reaction temperature = 90°C; 0.46 mg/L H_2S; 0.91 mg/L PH_3; 0.5% O_2.

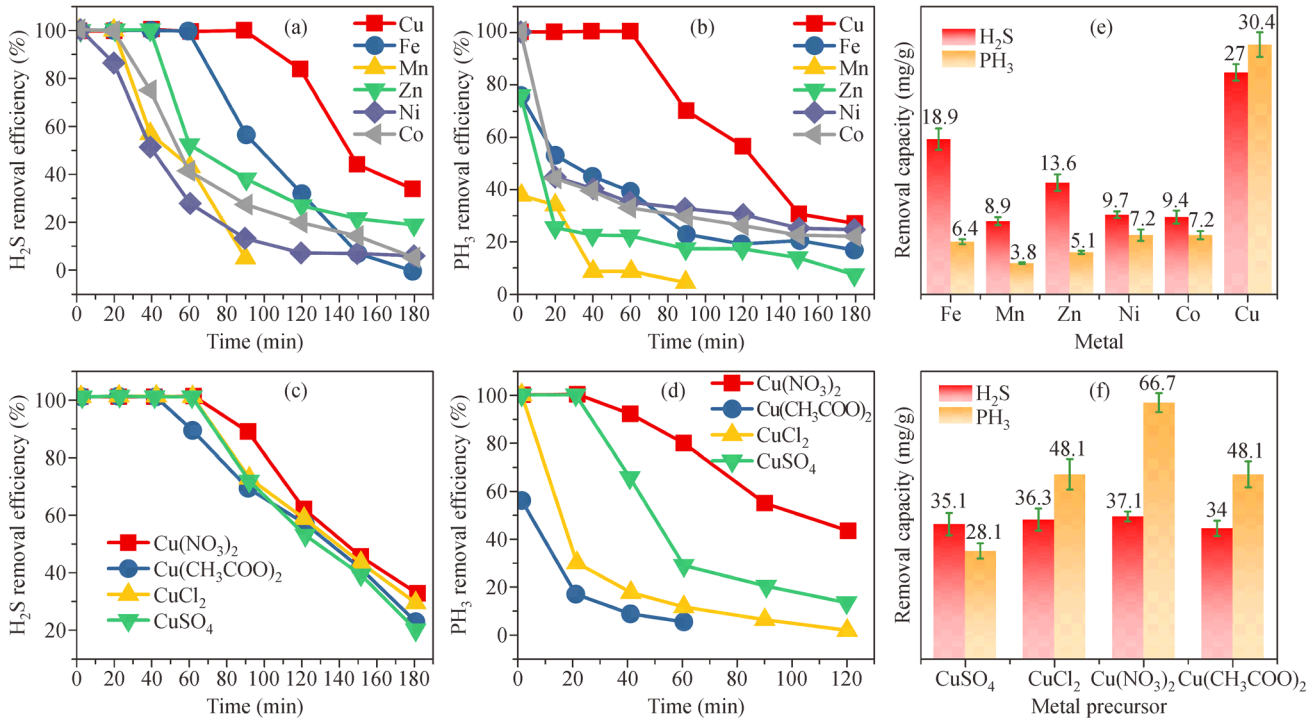

Fig. 2 The influence of transition metal and precursor on $M_{0.05}$/ACF for H_2S (a, c) and PH_3 (b, d) removal and their removal capacity (e, f). Conditions: 5% metal loading; reaction temperature = 90°C; calcination temperature = 550°C; 0.46 mg/L H_2S; 0.91 mg/L PH_3; 0.5% O_2.

growth to 119.6 mg/g for PH_3. The test results showed that the simultaneous removal capacity of H_2S and PH_3 by ACF could be dramatically improved via loading 15% Cu, which might be attributed to the good distribution of copper oxides on the ACF surface and much lower negative influence on the pore volume (Xu et al., 2017).

3.1.4 Influence of reaction temperature

The $Cu_{0.15}$/ACF has been used to discuss the influence of reaction temperature, which often affected the performance of catalysts. The calcination temperature has been fixed at 550°C. Figure 4 has shown the results and their capacity. As Figs. 4(a) and 4(b) demonstrated, the removal efficiency initially increased and then decreased with reaction temperature increasing. The $Cu_{0.15}$/ACF could show its best performance for H_2S and PH_3 simultaneous removal when the temperature was 90°C. For H_2S, the time for 100% removal of it was 300 min, which was 1.43 times than that of 25°C from Fig. 4(a). The removal capacity of H_2S increased by 64% with the reaction temperature rising from 25°C to 90°C from Fig. 4(c). At different reaction temperatures, the removal efficiency of PH_3 showed by the $Cu_{0.15}$/ACF is significantly different

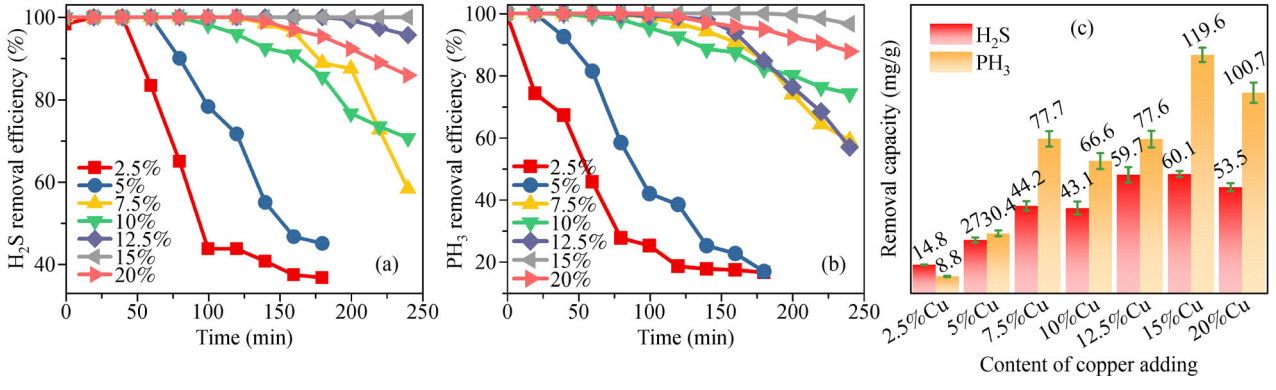

Fig. 3 The influence of Cu content on Cu_X/ACF for H_2S (a) and PH_3 (b) removal and their removal capacity (c). Conditions: reaction temperature = 90°C; calcination temperature = 550°C; 0.46 mg/L H_2S; 0.91 mg/L PH_3; 0.5% O_2.

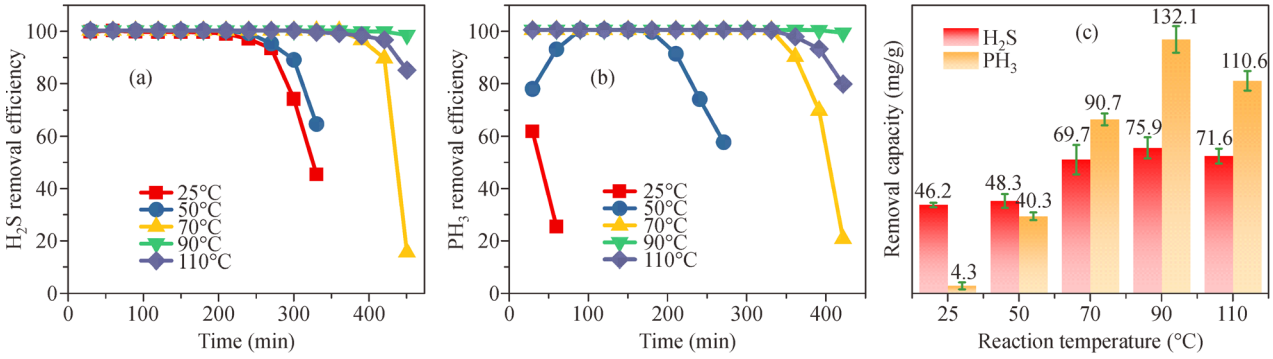

Fig. 4 The influence of reaction temperature on H_2S (a) and PH_3 (b) simultaneous removal by $Cu_{0.15}$/ACF and their removal capacity (c). Conditions: 15% metal (Cu) loading; calcination temperature = 550°C; 0.46 mg/L H_2S; 0.91 mg/L PH_3; 0.5% O_2.

from that of H_2S. Figure 4(b) displayed that it was difficult to achieve 100% instantaneous removal of PH_3 when the reaction temperature was lower than 70°C. This phenomenon was likely caused by insufficient catalyst activity. The duration of PH_3 100% removal was 240 min and the removal capacity of the $Cu_{0.15}$/ACF was dramatically promoted from 4.3 to 132.1 mg/g.

Otherwise, we noticed a decline in removal efficiency and removal capacity of $Cu_{0.05}$/ACF when the reaction temperature rose from 90°C to 110°C. This phenomenon could be explained as the activity of the active components of the catalyst might be promoted at high reaction temperature while the physical adsorption capacity of the carrier ACF was greatly weakened (Du, 2012; Zhang et al., 2015; Wang, 2016), which played a more critical role in the initial stage of the reaction process. Also, at higher reaction temperatures, H_2S and PH_3 could be separately oxidized to sulfate (SO_4^{2-}) and phosphate (PO_4^{3-}) more easily, and the higher concentration of them poisoned the catalysts (Sun et al., 2018; Wang et al., 2018). In summary, the test results suggested that the removal efficiency and capacity of H_2S and PH_3 could be greatly increased if the operating temperature is 90°C.

3.2 Discussion

3.2.1 XRD

XRD was used to analyze the surface species of Cu_x/ACF catalysts. Figure 5(a) showed the patterns of the catalysts prepared with different calcination temperatures. Figure 5 (b) displayed the patterns of catalysts with different copper adding.

From Fig. 5(a), the diffraction peak appeared around 22.7° could be found in all patterns, which belonged to C (JCPDS#50-0926). Comparing with the untreated ACF, new diffraction peaks were revealed, and some of them (35.6° and 38.1°) were attributed to cuprous oxide (Cu_2O) (JCPDS#05-0667) (Fuku, 2016). The rest peaks at 43.0°, 50.1°, and 73.9° were related to elemental copper (Cu) (JCPDS#04-0836). It can be seen from Fig. 5(a) that when the firing temperature is 450°C, Cu_2O is formed on the

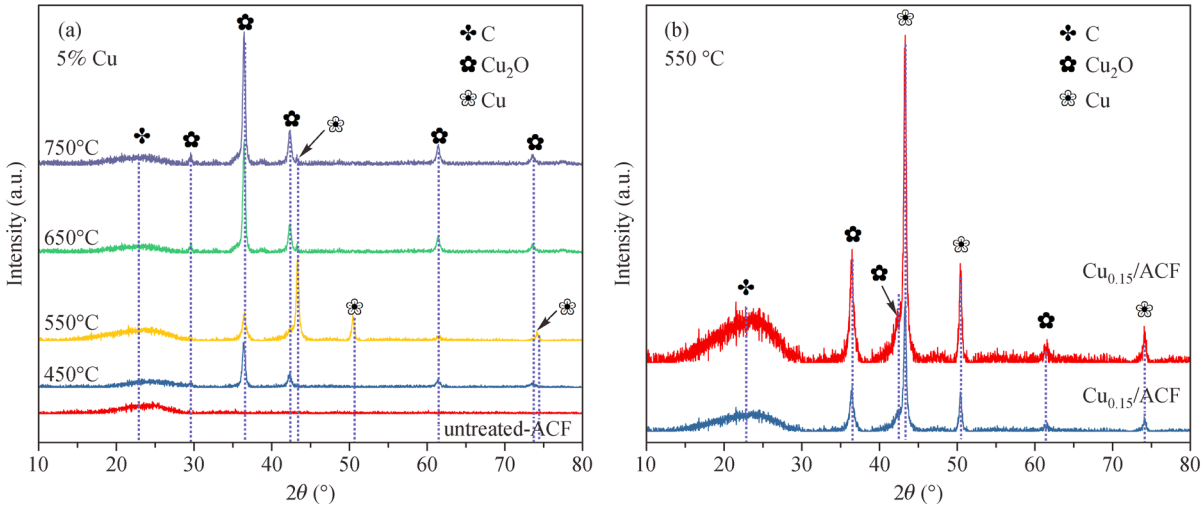

Fig. 5 XRD patterns of Cu_x/ACF catalysts: different calcination temperatures (a); different copper contents (b).

surface of ACF. When the temperature is 550°C, most of the Cu_2O is reduced to elemental Cu under the reduction of C. Raising the temperature to 650°C and 750°C, the elemental Cu disappeared and the Cu_2O formed again. References showed that the cuprous oxide could exist and growth at that temperatures (Du, 2012; Wang, 2016). This indicated that, at lower and higher temperatures, the Cu_2O was easily formed on the surface of the ACF in the presence of limited oxygen. At a relatively moderate temperature (around 550°C), elemental Cu was freely generated, which might be the main active component and helped the catalyst improve its performance. The crystal phase of copper (oxide) reflected by the XRD patterns was consistent with our experimental results, which was that the Cu-modified ACF calcinated at 550°C had the best results for H_2S and PH_3 simultaneous removal. Combined with the experimental and above analysis, it's clear that both Cu and Cu_2O can play a catalytic role, but the role of Cu is significantly higher than that of Cu_2O. This may be because elemental Cu has more active electric structure.

Figure 5 (b) presented the patterns of the $Cu_{0.050}$/ACF and $Cu_{0.150}$/AC. No new diffraction peaks appeared apart for the aforementioned. After increasing the amount of copper from 5% to 15%, there was a sharp rise in the intensity of the diffraction peaks, which could relate to the growth of crystal particles on the ACF. Hence, we analyzed the absolute crystallinity and grain size via Jade 6 to prove the above assumption (Table 1). The obtained absolute crystallinity of $Cu_{0.150}$/ACF was 56.3%, which was over double that of $Cu_{0.050}$/ACF (26.5%). The calculated grain size of Cu (1 1 1) on $Cu_{0.150}$/ACF separately were 9.0 nm, which became significantly larger than that of the $Cu_{0.050}$/ACF. Combined with the experimental results in part 3.1.3, the $Cu_{0.150}$/ACF performed much better for desulfurization and dephosphorization efficiency, indicating that it was more advantageous when the crystallinity and particle size of the active component elemental copper was higher.

3.2.2 SEM

The SEM was used to see surface morphology changes of the ACF after loading transition metal. Figure 6(a) to 6(g) represent the following: $Zn_{0.050}$/ACF, $Fe_{0.050}$/ACF, $Ni_{0.050}$/ACF, $Co_{0.050}$/ACF, $Mn_{0.050}$/ACF, $Cu_{0.050}$/ACF, and $Cu_{0.150}$/ACF.

By comparing the pictures between Fig. 6(a) and Fig. 6(f), it can be found that the dispersion state and crystal grains (size, uniformity, and quantity) of different metals (oxides) load on the surface of the ACF are very different, which may be related to the nature of the metal (oxides) itself and the binding ability of ACF. It is well known that the dispersibility and particles of the metal (oxide) on the carrier are closely related to its performance. After comparing the above pictures, it is clear that only copper (oxide) has good dispersibility and particle uniformity comparing with that of other metals (oxides). This may be one of the reasons why $Cu_{0.050}$/ACF performs better than other catalysts in H_2S and PH_3 removal (Kim et al., 2014).

Among the Fig. 6(f) and Fig. 6(g), the copper (oxide) disperses very well on both $Cu_{0.050}$/ACF and $Cu_{0.150}$/ACF. The main difference between them is that the crystal particles loaded on the $Cu_{0.15}$/ACF are significantly larger than that of $Cu_{0.050}$/ACF when increasing the content of Cu to 15%. This means that increasing a load of copper to a certain extent (15%) does not significantly change their dispersibility on the ACF, because they participate in the formation of larger particles of copper (oxide). This result can be supported by the previous XRD analysis results.

3.2.3 BET

The N_2 adsorption-desorption isotherms had been measured to explore the influences of different factors on the physical properties of the samples. Figure 7 showed their isotherms and pore size distribution, respectively. The

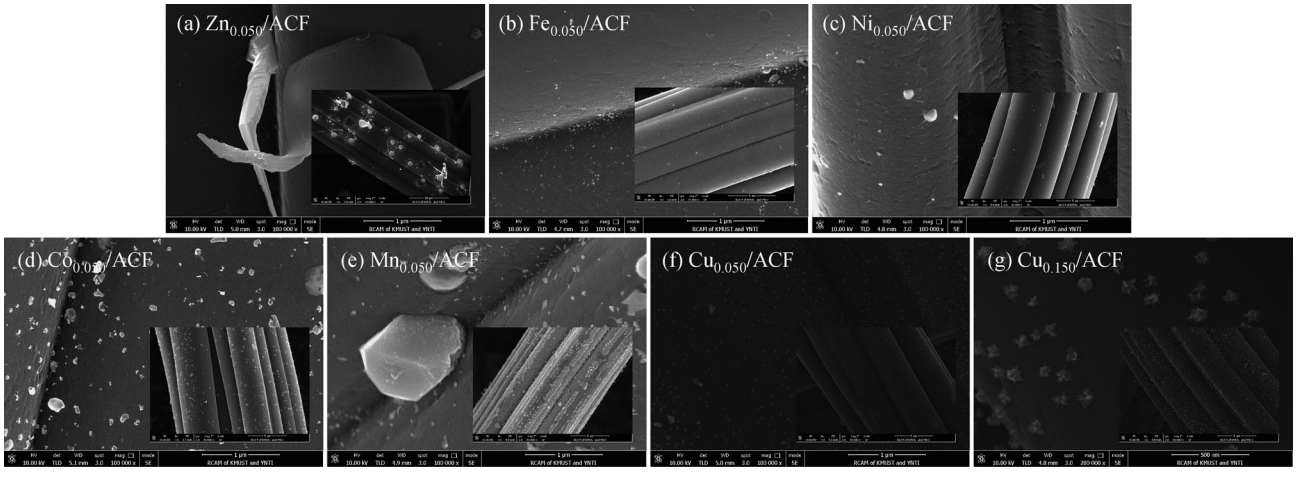

Fig. 6 SEM images of different catalysts. Conditions: (a–g) calcination temperature = 550°C, nitrate precursors; (a–f) 5% Cu loading; (g) 15% Cu loading.

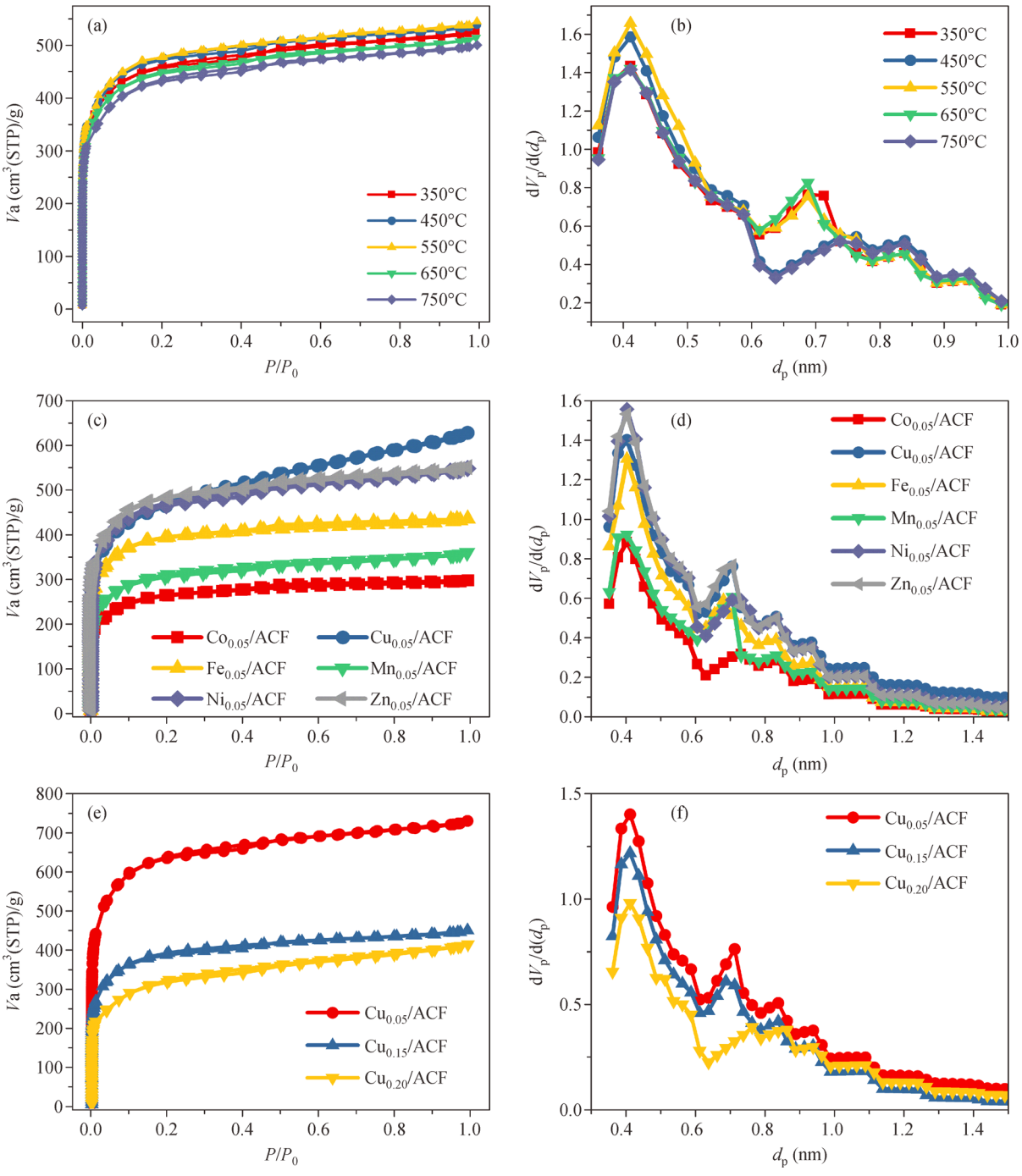

Fig. 7 The N_2 adsorption-desorption isotherms (a, c, e) and pore size distribution (b, d, f) of catalysts prepared under different conditions: (a, b) $Cu_{0.05}$/ACF; (c−f) calcination temperature = 550°C; nitrate precursors.

related physical property parameters were calculated based on the isotherms and the results had been listed in Table 1.

Figures 7(a) and 7(b) separately displayed the isotherms and pore size distribution of the catalysts prepared under different calcination temperatures. All isotherms belong to the I-type adsorption curve. The rapid increase of the adsorption amount in the low-pressure area indicated that the adsorbent belongs to the adsorption in the micropores and the adsorption content in the micropores was much higher than that of the surface (Gao et al., 2010). As the calcination temperature increases, their adsorption isotherms do not change much. However, Table 1 shows that the specific surface area (SSA), average pore size (APS), and total pore volume (TPV) of the catalyst calcined at 550°C are much better than that of other catalysts. This is one of the reasons for its better catalytic activity. Also, the

Table 1 The physical property parameters of different samples

Samples	SSA* (m^2/g)	APD *(nm)	TPV* (cm^3/g)
$Cu_{0.05}$/ACF@[350]	1748.3	0.62	0.81
$Cu_{0.05}$/ACF@[450]	1715.6	0.65	0.83
$Cu_{0.05}$/ACF@[550]	1768.9	0.57	0.96
$Cu_{0.05}$/ACF@[650]	1706.3	0.61	0.79
$Cu_{0.05}$/ACF@[750]	1660.1	0.58	0.77
Blank ACF	1791.9	1.73	1.03
$Fe_{0.05}$/ACF	1553.2	1.91	0.71
$Zn_{0.05}$/ACF	1302.3	1.02	0.92
$Co_{0.05}$/ACF	1001.5	1.96	0.43
$Ni_{0.05}$/ACF	1502.7	1.57	0.79
$Mn_{0.05}$/ACF	1159.8	1.82	0.63
$Cu_{0.05}$/ACF	1768.6	0.57	0.96
$Cu_{0.15}$/ACF	1487.4	0.53	0.69
$Cu_{0.20}$/ACF	980.8	0.38	0.51

Notes: SSA*: Specific surface area; APD*: Average pore diameter; TPV*: Total pore volume.

specific surface area of the catalyst prepared under high-temperature conditions decreased significantly, which was probably caused by the agglomeration of surface metal (oxide) blocking part of the pores. This can be explained by the analysis content of the XRD part. From Fig. 3(b), it could represent that the pore size of the catalysts are mainly distributed around 0.42 nm and 0.69 nm.

Figures 7(c) and 7(d) presented the isotherms and pore size distribution of the catalysts loaded by different metals (oxide). Similar to the previous ones, the isotherms are all I-type, which is microporous adsorption. The adsorption amount of the catalyst supported by copper (oxide) was slightly higher than that of other catalysts. Combining the data in Table. 1, it can be determined that its SSA and TPV are 1768.6 m^2/g and 0.96 cm^3/g, respectively. They are slightly lower than that of the blank ACF but much higher than others. This is due to the good dispersibility of copper (oxide) on the ACF, which can be supported by the analysis results of the SEM part. Furthermore, the pore size distribution is consistent with the previous analysis.

Figures 7(e) and 7(f) showed the isotherms and pore size distribution of the catalysts loaded by different copper amounts. The pore distribution and the type of adsorption isotherms and pore are consistent with the previous analysis. Figure 7(a) reflects that gradually increasing the added copper amount will result in a sharp drop in the adsorption amount of the catalysts. Some pores are blocked. This is an issue that cannot be avoided while adding a large amount of copper to enhance the activity of the catalysts. From the data in Table 1, it can be seen more intuitively that as the loading content of copper increases, the SSA and TPV of the corresponding catalysts drop sharply. In combination with the experimental results, the $Cu_{0.15}$/ACF has the best effect in removing H_2S and PH_3 at the same time, indicating that loading 15% copper into ACF can greatly enhance the activity of the catalyst and can take advantage of the large SSA of ACF.

4 Analysis of the deactivation theory

Based on the $Cu_{0.150}$/ACF, we explored the reaction process by analyzing its changes before and after the reaction. The reaction conditions were the same as the experimental conditions. *In situ* IR spectra, the results have been shown in Fig. 8.

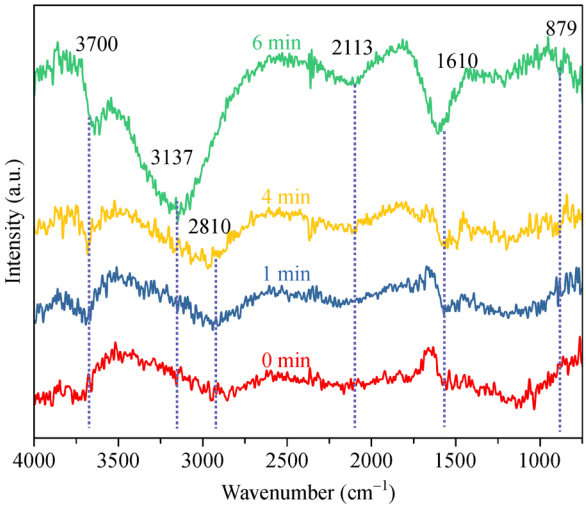

Fig. 8 *In situ* IR spectrogram of $Cu_{0.15}$/ACF. Conditions: calcination temperature = 550°C; 15% Cu loading; nitrate precursors.

The peak that occurred in 3740 cm^{-1} was H-O-H(Naito et al., 2006), which slightly increased as the reaction progress. Combining with the peaks around 1700 cm^{-1} ($[SO_4^{2-}(H_2O)_6]$ (Zhou et al., 2006)), and 2548−3700 cm^{-1} ($CO_3^{2-}\cdot nH_2O(n = 5–7)$ (Pathak and Maity, 2009)), it could be inferred that lots of water was formed during the reaction and then involved in the formation of a specific sulfate and carbonate. This phenomenon was also consistent with the water droplets we found on the inner wall of the reactor during our experiments. The peak at 2120 cm^{-1} was assigned to-NH_2 groups derived from HNO_3 which may generate in the calcination process and it could show a strong oxidizing property, which might help to oxidize H_2S and PH_3. The peak at 879 cm^{-1} was $H_2PO_4^-$ (Klähn et al., 2004), indicating there was deep oxidation for PH_3 according to the valence state of P. Based on the above analysis, we boldly presented the reaction process which has been displayed in Fig. 9. Under the power of active sites (Cu and CuO) and-NH_2 groups, the PH_3 transferred to $H_2PO_4^-$ and H_2O (1) with O_2. H_2S turned to SO_4^{2-} and H_2O (2). Finally, all of the H_2O participated in the formation of $[SO_4^{2-}(H_2O)_6]$. The possible reaction equations were as follows:

$$4PH_3 + 9O_2 \rightarrow 2H_2O + 4H_2PO_4^- \quad (3)$$

$$2H_2S + 5O_2 \rightarrow 2SO_4^{2-} + 2H_2O \quad (4)$$

$$SO_4^{2-} + 6H_2O \rightarrow SO_4^{2-}(H_2O)_6 \quad (5)$$

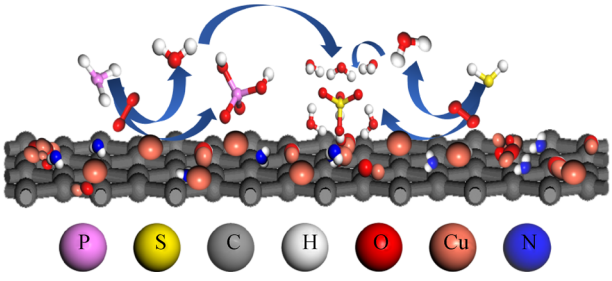

Fig. 9 The reaction process.

5 Conclusions

The Cu modified ACF was fabricated for H_2S and PH_3 simultaneous removal at low temperatures. Based on the experimental results, the ACF after loading 15% Cu achieved the highest performance with a removal capacity of 75.9 mg/g and 132.1 mg/g for H_2S and PH_3, respectively. Also, the 550°C and 90°C were the suitable calcination and reaction temperature. The 550°C is good for the formation of the copper element on the surface of ACF, and lower or higher temperature will generate more cuprous oxide. The role of the former is significantly greater than that of the latter. Besides, the ACF can still maintain the advantages of larger specific surface area and pore volume after loading copper due to the good dispersibility of copper (oxide), which is the main reason for the better performance of $Cu_{0.150}$/ACF. Increasing the copper loading content can significantly promote the crystallinity and particle size of copper (oxide) on the ACF, thereby improving its catalytic performance. Finally, *in situ* IR characterization results gave the deactivation reasons for the catalyst. It was the accumulation of $H_2PO_4^-$ and $SO_4^{2-}(H_2O)_6$, which were from the oxidation of PH_3 and H_2S, respectively. Certainly, additional research should follow this work, such as regeneration and deeper reaction processes.

Acknowledgements This work was supported by the National Natural Science Foundation of China (Nos. 51968034, 41807373 and 22006058), the National Key R&D Program of China (No. 2018YFC0213400), and the Science and Technology Program of Yunnan Province (No. 2019FB069).

Electronic Supplementary Material Supplementary material is available in the online version of this article at https://doi.org/10.1007/s11783-021-1425-3 and is accessible for authorized users.

References

Abdolghaffari A H, Baghaei A, Solgi R, Gooshe M, Baeeri M, Navaei-Nigjeh M, Hassani S, Jafari A, Rezayat S M, Dehpour A R, Mehr S E, Abdollahi M (2015). Molecular and biochemical evidences on the protective effects of triiodothyronine against phosphine-induced cardiac and mitochondrial toxicity. Life Sciences, 139: 30–39

Bai B C, Lee C W, Lee Y S, Im J S (2017). Modification of textural properties of CuO-supported activated carbon fibers for SO_2 adsorption based on electrical investigation. Materials Chemistry and Physics, 200: 361–367

Basova Y V, Edie D D, Badheka P Y, Bellam H C (2005). The effect of precursor chemistry and preparation conditions on the formation of pore structure in metal-containing carbon fibers. Carbon, 43(7): 1533–1545

de Falco G, Montagnaro F, Balsamo M, Erto A, Deorsola F A, Lisi L, Cimino S (2018). Synergic effect of Zn and Cu oxides dispersed on activated carbon during reactive adsorption of H_2S at room temperature. Microporous and Mesoporous Materials, 257: 135–146

Deng J, Chen L, Wei W (2013). The study on removal the PH_3 in CO by Dephosphorization bacteria. Advanced Materials Research, 781: 861–868

Du J (2012). Growth of single-crystalline Cu_2O (111) film on ultrathin MgO modified α-Al_2O_3 (0001) substrate by molecular beam epitaxy. Journal of Crystal Growth, 353(1): 63–67

Fuku X, Kaviyarasu K, Matinise N, Maaza M. (2016). Punicalagin green functionalized Cu/Cu_2O/ZnO/CuO nanocomposite for potential electrochemical transducer and catalyst. Nanoscale Research Letters, 11(1): 386

Gao F, Zhao D L, Li Y, Li X G, Solids C O (2010). Preparation and hydrogen storage of activated rayon-based carbon fibers with high

specific surface area. Journal of Physics, 71(4): 444–447

Gu T, Gao F, Tang X, Yi H, Zhao S, Zaharaddeen S, Zhang R, Zhuang R, Ma Y J E S (2019). Fe-modified Ce-MnO_x/ACF N catalysts for selective catalytic reduction of NO_x by NH_3 at low-middle temperature. Environmental Science and Pollution Research International, 26(27): 27940–27952

Hou Y, Li Y, Li Q, Liu Y, Huang Z (2019). Insight into the role of TiO_2 modified activated carbon fibers for the enhanced performance in low-temperature NH_3-SCR. Fuel, 245: 554–562

Kim J, Lee B K (2018). Enhanced photocatalytic decomposition of VOCs by visible-driven photocatalyst combined Cu-TiO_2 and activated carbon fiber. Process Safety and Environmental Protection, 119: 164–171

Klähn M, Mathias G, Kötting C, Nonella M, Schlitter J, Gerwert K, Tavan P (2004). IR spectra of phosphate ions in aqueous solution: predictions of a DFT/MM approach compared with observations. The Journal of Physical Chemistry A, 108(29): 6186–6194

Lan H, Wang A, Liu R, Liu H, Qu J (2015). Heterogeneous photo-Fenton degradation of acid red B over Fe_2O_3 supported on activated carbon fiber. Journal of Hazardous Materials, 285: 167–172

Lee T, Ooi C H, Othman R, Yeoh F Y (2014). Activated carbon fiber-the hybrid of carbon fiber and activated carbon. Reviews on Advanced Materials Science, 36(2): 118–136

Li S, Li K, Hao J, Ning P, Tang L, Sun X (2016). Acid modified mesoporous Cu/SBA-15 for simultaneous adsorption/oxidation of hydrogen sulfide and phosphine. Chemical Engineering Journal, 302: 69–76

Liu D, Li B, Wu J, Liu Y (2020). A review on sorbents for hydrogen sulfide capture from biogas at low temperature. Environmental Chemistry Letters, 18: 113–128

Ma L, Ning P, Zhang Y, Wang X (2008). Experimental and modeling of fixed-bed reactor for yellow phosphorous tail gas purification over impregnated activated carbon. Chemical Engineering Journal, 137 (3): 471–479

Naito S, Aida S, Kasahara T, Miyao T (2006). Infrared spectroscopic study on the reaction mechanism of CO hydrogenation over Pd/CeO_2. Research on Chemical Intermediates, 32(3−4): 279–290

Ma Y, Wang X, Ning P, Cheng C, Wang F, Wang L, Lin Y, Yu Y, Fuels (2016). Simultaneous removal of PH_3, H_2S, and dust by corona discharge. Energy, 30(11): 9580–9588

Pathak A, Maity D (2009). Distinctive IR signature of CO_3^- and CO_3^{2-} hydrated clusters: A theoretical study. The Journal of Physical Chemistry A, 113(48): 13443–13447

Stita S, Galera Martínez M, Pham Xuan H, Pham Minh D, Nzihou A, Sharrock P (2015). Metal-doped apatitic calcium phosphates: Preparation, characterization, and reactivity in the removal of hydrogen sulfide from gas phase. Composite Interfaces, 22(6): 503–515

Sun L, Song X, Li K, Wang C, Sun X, Ning P, Huang H (2020). Preparation of modified manganese slag slurry for removal of hydrogen sulphide and phosphine. Canadian Journal of Chemical Engineering, 98(7): 1534–1542

Sun X, Ruan H, Song X, Sun L, Li K, Ning P, Wang C (2018). Research into the reaction process and the effect of reaction conditions on the simultaneous removal of H_2S, COS and CS_2 at low temperature. RSC Advances, 8(13): 6996–7004

Wang F (2016). Effect of annealing process on the heterostructure CuO/Cu_2O as a highly efficient photocathode for photoelectrochemical water reduction. Journal of Physics and Chemistry of Solids, 104: 139–144

Wang Y, Lin Q, Ning P, Wang C, Sun X, Li K (2018). Preparation of $Ce_{0.6}$-Cu_{60}/Al_{40}-[O] catalyst and role of CeO_2/CuO in simultaneous removal of H_2S and PH_3. Journal of the Taiwan Institute of Chemical Engineers, 87: 44–53

Xu W, Chen B, Jiang X, Xu F, Chen X, Chen L, Wu J, Fu M, Ye D (2020). Effect of calcium addition in plasma catalysis for toluene removal by Ni/ZSM-5: Acidity/basicity, catalytic activity and reaction mechanism. Journal of Hazardous Materials, 387: 122004

Xu X, Huang G, Qi S (2017). Properties of AC and 13X zeolite modified with $CuCl_2$ and $Cu(NO_3)_2$ in phosphine removal and the adsorptive mechanisms. Chemical Engineering Journal, 316: 563–572

Zhang X, Tang Y, Qu S, Da J, Hao Z (2015). H_2S-selective catalytic oxidation: Catalysts and processes. ACS Catalysis, 5(2): 1053–1067

Zhao B, Yi H, Tang X, Li Q, Liu D, Gao F (2016). Copper modified activated coke for mercury removal from coal-fired flue gas. Chemical Engineering Journal, 286: 585–593

Zhou J, Santambrogio G, Brümmer M, Moore D T, Wöste L, Meijer G, Neumark D M, Asmis K R (2006). Infrared spectroscopy of hydrated sulfate dianions. The Journal of Chemical Physics, 125: 111102